Available online at www.sciencedirect.com

SciVerse ScienceDirect

journal homepage: www.elsevier.com/locate/he

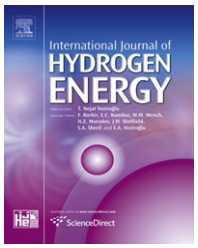

Experimental and numerical investigation on combustion characteristics of premixed hydrogen/air flame in a micro-combustor with a bluff body

Jianlong Wan [a], *Aiwu Fan* [a,*], *Kaoru Maruta* [b], *Hong Yao* [a], *Wei Liu* [a]

[a] *State Key Laboratory of Coal Combustion, Huazhong University of Science and Technology, 1037 Luoyu Road, Wuhan 430074, China*
[b] *Institute of Fluid Science, Tohoku University, Sendai 980-8577, Japan*

ARTICLE INFO

Article history:
Received 23 August 2012
Received in revised form
23 September 2012
Accepted 25 September 2012
Available online 25 October 2012

Keywords:
Micro-combustor
Bluff body
Blow-off limit
Exhaust gas temperature
Combustion efficiency

ABSTRACT

Combustion characteristics of lean hydrogen/air mixture in a planar micro-channel with a bluff body were investigated experimentally and numerically. Effects of the inlet velocity and equivalence ratio on the blow-off limit, combustion efficiency and exhaust gas temperature were examined. The results show that the blow-off limit is greatly extended as compared with that of the micro-combustor without a bluff body. Moreover, the blow-off limit increases as the equivalence ratio is increased from 0.4 to 0.6. Furthermore, with the increase of inlet velocity, the flame front is prolonged and becomes narrower, and the high temperature segment of outer wall shifts downstream. In addition, the combustion efficiency and exhaust gas temperature increase first and then decrease with the increase of the inlet velocity. Finally, comparatively high combustion efficiency can be maintained over the whole combustible velocity range at a moderate equivalence ratio.

1. Introduction

With the rapid progresses of micro-electro-mechanic system (MEMS) technology, various small devices and systems, including micro-aircrafts, robots, gas turbines, engines and portable electronic and communication devices, are continuously emerging for military, industrial applications and human daily lives [1]. Conventional batteries cannot act as power sources satisfactorily for those small devices because batteries are heavy, and have a low energy density, a short duration as well as a long recharging time. Combustion-based micro-power-generation devices and systems are considered to be one of the competitive alternatives due to the much higher energy densities of hydrocarbon fuels as compared with those of conventional electrochemical batteries [2-4].

Meanwhile, there are several challenges we have to take up in developing micro-combustors [2]. One of the most important issues is the increased heat losses due to the large surface area-to-volume ratio of the micro-combustor [2]. Another critical problem is the shortened residence time of the gaseous mixture under reduced dimension. Many researchers have made tremendous contributions to the study of flame stability of premixed combustion under small scales. For instance, Maruta et al. [5] investigated the combustion behavior of premixed CH_4/air mixtures in a heated quartz tube with a 2.0-mm diameter. Flames with repetitive extinction and ignition (FREI) were observed with a high-speed video camera. Later, similar flame dynamics were confirmed and interpreted by many other researchers [6–10]. For example, Pizza et al. [8] numerically investigated the combustion characteristics of hydrogen/air

* *Corresponding author*. Tel.: +86 27 87542618; fax: +86 27 87540724.
E-mail address: faw@mail.hust.edu.cn (A. Fan).
0360-3199/$ – see front matter
http://dx.doi.org/10.1016/j.ijhydene.2012.09.154

mixture in a heated planar micro-channel. Their results demonstrated that the stable combustion region was very limited. After that, Minaev et al. [11] predicted that flame splitting phenomenon exists in micro-channel with constant wall temperature profile. Fan et al. [12] confirmed this prediction through experiment. Very recently, Nakamura et al. [13] numerically investigated the flame splitting phenomenon during the FREI processes. This work successfully revealed the details of the multiple ignition kernels in the flow reactor. Flame instabilities in a radial micro-channel were systematically investigated by Kumar et al. [14,15] and Fan et al. [16,17]. In addition to stable circular flame, a variety of non-stationary flame patterns, such as the rotating Pelton-wheel-like flames, traveling flames, spiral-like flame, and so forth, were observed. Stability of premixed hydrogen-air flame in radial micro-channel was investigated experimentally and numerically by Zamashchikov and Tikhomolov [18].

Great efforts have been made to improve flame stability in micro- and meso-scale combustors. Thermal managements, such as heat recirculation, are frequently adopted in the design of small combustors. For instance, the "Swiss Roll" structure has been implemented to stabilize flames in micro- and meso-scale burners [19]. Jejurkar and Mishra studied flame stability in an annular micro-combustor [20]. Li et al. [21] developed a planar micro-combustor fitted with stainless steel mesh. It was shown that flame was effectively anchored by the inserted porous media. Jiang et al. [22] proposed a miniature cylindrical combustor with porous wall. Flame can be stabilized in the combustor chamber due to the reduction of heat losses and preheating effect of the fresh mixture. Another way to anchor flame in micro-combustors is to form a flow recirculation zone. For an example, Yang et al. [23] and Pan et al. [24] made a comparative study on the combustion in micro-cylindrical combustors with and without a backward facing step. Their work showed that the step was very useful in controlling flame position and widening the operational range of flow rate. Many other researchers adopted catalysts in micro-combustor for flame stabilization [25–30].

Although a variety of flame stabilization approaches have been reported in the literature, simple yet effective methods are still desirable to widen the stable operating range of combustion-based micro-power generation systems. It is well known that bluff bodies are extensively used for flame stabilization in various industrial combustion and propulsion systems [31]. However, their applications to micro-combustors have not been reported to date. Thus, in the present work, we developed a planar micro-combustor with a bluff body to extend the stable combustion region of premixed H_2/air flame in micro-channels. Combustion characteristics of lean premixed H_2/air flame in this combustor were studied experimentally and numerically. The blow-off limit and exhaust gas temperature were investigated through experiment, while some other characteristics were explored via numerical simulation due to the inconvenience of measurement.

2. Experimental setup and method

The geometric diagram of the planar micro-combustor is schematically shown in Fig. 1. The total length (L_0) is 16 mm and the thickness of combustor wall (W_3) is 1 mm. The width (W_0) and height (W_1) of the combustor chamber are 10 mm and 1 mm, respectively. The cross-section of the bluff body is an equilateral triangle with a side length (W_2) of 0.5 mm. The bluff body is symmetrically located with respect to the combustor walls, and the distance from its vertical surface to the combustor inlet (L_1) is 1 mm. Both of the combustor wall and bluff body are made of quartz glass which can endure a very high temperature.

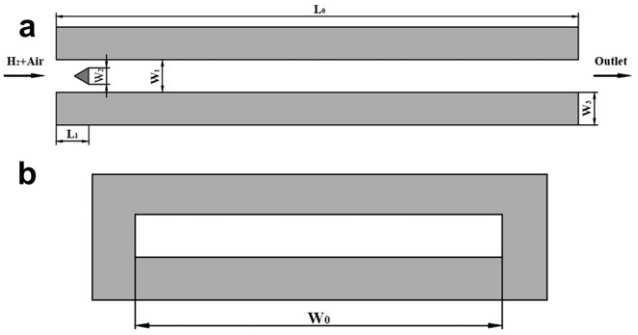

Fig. 1 – Schematic diagram of the micro combustor with a bluff body: (a) cross section of the combustor, (b) combustor exit.

The experimental system is shown in Fig. 2. Hydrogen and air of high pressure were stored in two gas tanks. Their pressures were reduced to atmospheric pressure by using pressure reducing valves, while the mass flow rates were adjusted and controlled by electric mass flow meters with an accuracy of 1% over the full range. The fuel and air streams were fully mixed in a mixer before entering into the micro-combustor. An electric spark igniter is applied to ignite the fresh mixture. For the sake of safety, a flash arrester was used between the mixer and the flow meter of hydrogen. Moreover, a K-type thermocouple with a bead diameter of 0.5 mm was used to measure the exhaust gas temperature, and the temperature presented in this paper has been corrected considering the heat losses to the ambient [32]. A digital camera was used to take flame pictures from the top viewpoint.

At the beginning of the combustion experiment, we first ignite the fuel/air mixture at a low velocity under which flame can be stabilized behind the bluff body, and then increase the inlet velocity with a step of 1.0 m/s, until the flame is blown out of the micro-combustor. The largest inlet velocity was decided as the blow-off limit. The above procedure is adopted for all the cases with different equivalence ratios.

Because the size of combustor exit was too small to sample the exhaust gas, the analysis of exhaust gas was not carried out and the combustion efficiency was obtained through numerical simulation.

3. Numerical model

3.1. *Governing equations*

As the characteristic length of the combustor chamber is still sufficiently larger than the molecular mean-free path of gases flowing through the micro-combustor, fluids can be reasonably

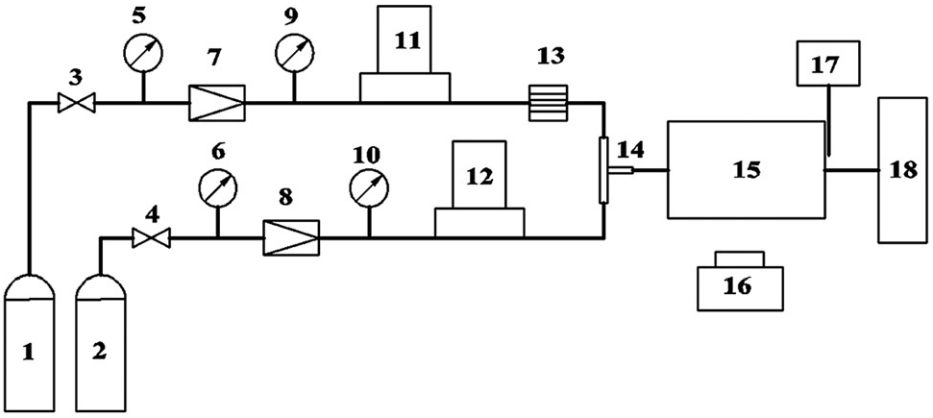

1-Hydrogen cylinder; 2-Air cylinder; 3,4-Manual valves; 5,6,9,10-Pressure gauges; 7,8-Pressure reducing valves; 11,12- Mass flow controller; 13- Flash arrester; 14-Mixer; 15-Micro combustor; 16- Digital camera; 17- Electric spark igniter; 18- Thermocouple;

Fig. 2 – Schematic diagram of the experimental system.

considered as continuums and the Navier–Stokes equations are still suitable in the present study. Kuo and Ronney [33] reported that it is more appropriate to predict the combustion characteristics in micro-combustors by using a turbulence model when the Reynolds number is above ~500. It is expected that in a micro-combustor, the mixing of various kinds of species is enhanced due to the small space. The turbulence model is better than the laminar model to reflect the enhanced mixing and its effect on combustion characteristics. In our case, the corresponding inlet velocity for $Re = 500$ is ~8.0 m/s. As the main purpose of the micro-combustor fitted with a bluff body is to extend the blow-off limit, which is much larger than 8.0 m/s (refer to subsection 4.2), therefore, the realizable $k-\varepsilon$ turbulence model is adopted here. Our experimental results also validate the suitability of this model for the present work, which will be shown in the subsection 4.2. The governing equations for the gaseous mixture are shown below [34]:

Continuity:

$$\frac{\partial}{\partial x}(\rho v_x) + \frac{\partial}{\partial y}(\rho v_y) = 0 \tag{1}$$

Momentum:

$$\text{X direction}: \quad \frac{\partial(\rho v_x v_x)}{\partial x} + \frac{\partial(\rho v_x v_y)}{\partial y} = -\frac{\partial p}{\partial x} + \frac{\partial \tau_{xx}}{\partial x} + \frac{\partial \tau_{xy}}{\partial y} \tag{2}$$

$$\text{Y direction}: \quad \frac{\partial(\rho v_y v_x)}{\partial x} + \frac{\partial(\rho v_y v_y)}{\partial y} = -\frac{\partial p}{\partial y} + \frac{\partial \tau_{yx}}{\partial x} + \frac{\partial \tau_{yy}}{\partial y} \tag{3}$$

Energy:

$$\frac{\partial(\rho v_x h)}{\partial x} + \frac{\partial(\rho v_y h)}{\partial y} = \frac{\partial(k_f \partial T)}{\partial x^2} + \frac{\partial(k_f \partial T)}{\partial y^2} + \sum_i \left[\frac{\partial}{\partial x}\left(h_i \rho D_{i,m} \frac{\partial Y_i}{\partial x}\right) + \frac{\partial}{\partial y}\left(h_i \rho D_{i,m} \frac{\partial Y_i}{\partial y}\right)\right] - \sum_i h_i R_i \tag{4}$$

Species:

$$\frac{\partial(\rho Y_i v_x)}{\partial x} + \frac{\partial(\rho Y_i v_y)}{\partial y} = -\left[\frac{\partial}{\partial x}\left(\rho D_{i,m} \frac{\partial Y_i}{\partial x}\right) + \frac{\partial}{\partial y}\left(\rho D_{i,m} \frac{\partial Y_i}{\partial y}\right)\right] + R_i \tag{5}$$

where ρ (kg/m^3) is density; v_x (m/s) and v_y (m/s) are the velocity components in the x and y directions, respectively; p (Pa) is pressure; τ (Pa) is shear stress; h_i (J/kg) is the enthalpy of species i; k_f (W/m K) is the thermal conductivity of fluid; T (K) is temperature; Y_i (kg/kg) denotes the mass fraction of species i; R_i (kg/s m^3) is the generation or consumption rate of species i; D_{im} (m^2/s) is the mass diffusivity of species i.

As has been shown by many researches that heat conduction in the solid phase exerts an important effect on the combustion [18–20,33], we consider the heat transfer in both combustor walls and bluff body in the computation. The energy equation for the solid phase is given as:

$$\frac{\partial(k_s \partial T)}{\partial x^2} + \frac{\partial(k_s \partial T)}{\partial y^2} = 0 \tag{6}$$

where k_s (W/m K) is the thermal conductivity of solid material.

3.2. *Computation scheme*

Because hydrogen has much higher burning velocity than other hydrocarbon fuels, we select it as the fuel in the present study. To protect the bluff body and combustor walls against too high temperatures, lean mixtures with equivalence ratios of 0.4, 0.5 and 0.6 are used to control the maximal temperature. The equivalence ratio, ϕ, is a commonly used index to indicate quantitatively whether the fuel-air mixture for a chemical reaction is rich ($\phi > 1$), lean ($\phi < 1$), or stoichiometric ($\phi = 1$). The equivalence ratio is defined as [34]

$$\phi = \frac{(F/A)}{(F/A)_{stoic}} \tag{7}$$

where (F/A) and $(F/A)_{stoic}$ are the real and stoichiometric **mass** ratios of the fuel (F) to the air (A).

The density of the gas mixture is calculated using the ideal gas assumption, while the specific heat, viscosity, and thermal conductivity are calculated from a mass fraction weighted average of species properties [35]. Temperature dependence of

all the required physico-chemical parameters is incorporated using polynomial functions based on handbook values [36].

The reaction mechanism reported by Li et al. [37] is applied to model the combustion of H_2/air mixtures. It consists of 19 reversible elementary reactions and 13 species. Detailed transport properties of the gaseous mixture are computed using the CHEMKIN database [38]. The laminar finite-rate model is selected to solve the interaction between turbulence flow and combustion. As the micro-combustor has been processed via special measures which made all the surfaces inert, the surface reaction effect was not considered in CFD simulation.

Uniform concentration and velocity distributions of premixed H_2/air mixture are specified at the inlet of micro-combustor. The inlet temperature of mixture is set at 300 K. At the exit, a pressure outlet boundary condition is specified with a pressure of 1.013×10^5 Pa. Surface to surface radiation between the inner surfaces of the combustor is considered using the discrete ordinates (DO) model [33]. At the inner wall, boundary conditions of non-slip and no species flux normal to the wall surface are applied. At the outer surface of the solid walls, heat losses to the surroundings are calculated through Eq. (8), in which both natural convection and thermal radiation are considered. α is the natural convection heat transfer coefficient and we give it a constant value of 20 W/m^2/K [39]. $T_{w,o}$ is the outer wall temperature and T_∞ is the ambient temperature. The ambient temperature is about 25 °C (298 K) during the experiment. For simplicity, we used a constant value of 300 K in the computation. The error by doing this is negligible. ε is the emissivity of the solid surface, and σ is the Stephan–Boltzmann constant, with a value of 5.67×10^{-8} W/(m^2 K^4).

$$q = \alpha(T_{w,o} - T_\infty) + \varepsilon\sigma\left(T_{w,o}^4 - T_\infty^4\right) \quad (8)$$

FLUENT 6.3 [40] is applied to solve the conservation equations of mass, momentum, energy and species as well as the conjugated heat conduction in solid materials. The second-order upwind scheme was used for discretization and the "SIMPLE" algorithm was employed for the pressure–velocity coupling. As can be seen from Fig. 1b, the aspect ratio ($W_1/W_0 = 1{:}10$) of the combustor chamber is very small, therefore, a two-dimension, steady-state solver is selected to reduce the computation load. Grid-independence of the results was verified and a non-uniform square grid system with 171,132 cells was employed in the final computation. The convergence of CFD simulation is judged upon residuals of all governing equations. Results reported here were achieved with residuals smaller than 1.0×10^{-6}.

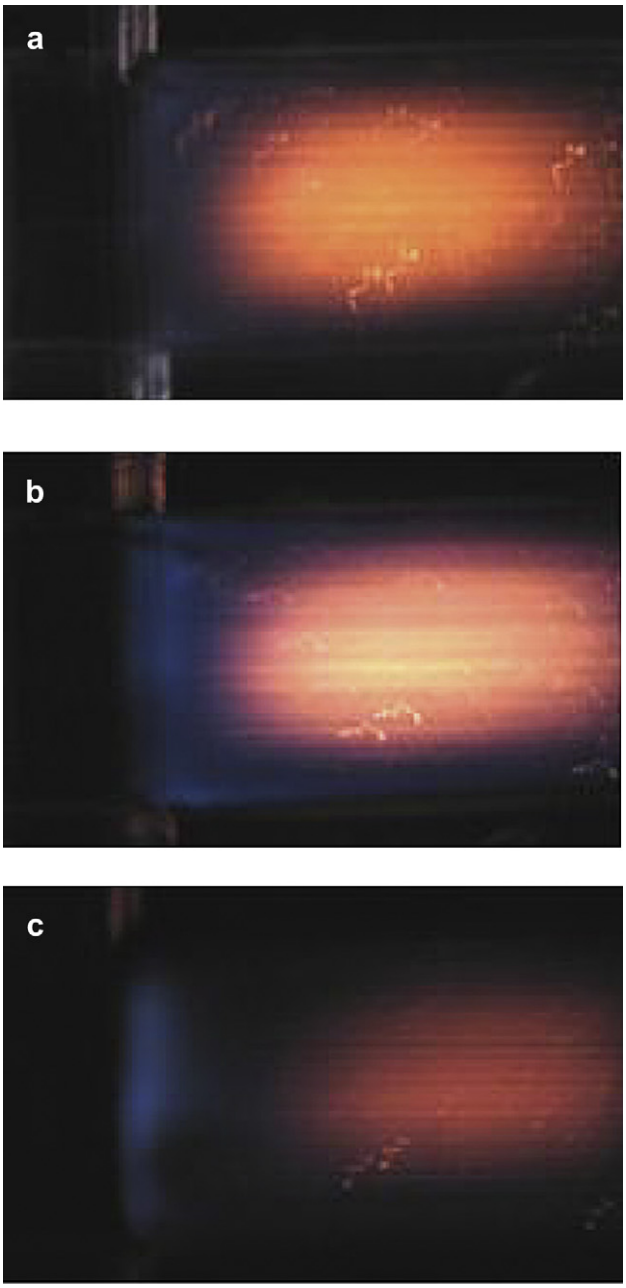

Fig. 3 – Flame photos for different inlet velocities at the same equivalence ratio of 0.5: (a) V_{in} = 15 m/s, (b) V_{in} = 23 m/s, (c) V_{in} = 40 m/s. The inlet of the combustor is on the left side.

4. Results and discussion

4.1. Flame observation

Flame pictures were taken with a still digital camera from the top viewpoint at each inlet velocity. Here, we only present three photos at 15, 23 and 40 m/s for the equivalence ratio of 0.5, as shown in Fig. 3. This is because they can show the typical variation tendency of the flame appearance. As the tendency is similar under other equivalence ratios, it is no need to present flame pictures of all cases. From Fig. 3a it is seen that when the inlet velocity is 15 m/s, flame can be stabilized behind the bluff body, and the color of the combustor wall is red (in the web version). As the inlet velocity is increased to 23 m/s, the high temperature zone is gradually shifted downstream and looks even brighter (Fig. 3b), indicating a higher flame temperature. With a further increment of the inlet velocity to 40 m/s, the high temperature zone is pushed to even farther downstream, and the color of combustor wall becomes dark red, which can be clearly seen

in Fig. 3c. Thus, the combustion has deteriorated in this case, i.e., it is a condition near the blow-off limit.

4.2. *Blow-off limit*

The experimental results of blow-off limits under different equivalence ratios have been obtained through both experimental investigation and numerical simulation, as shown in Fig. 4. It can be seen from Fig. 4 that the predicted blow-off limits agree reasonably well with the counterparts of the experiment. The relative errors between the numerical and experimental results are 5.3%, 12.2% and 5.8% for the equivalence ratios of 0.4, 0.5 and 0.6, respectively. This confirms the reasonable accuracy of the numerical model adopted in the present paper. To further validate the suitability of the turbulence model, we also conducted numerical simulation with the laminar model. For example, when the equivalence ratio is 0.5, the blow-off limit computed with the laminar model is only 16 m/s, which is much less than both the experimental data (41 m/s) and computation result with the turbulence model (36 m/s).

For the planar micro-combustor without a bluff body, the blow-off limits are about 3.0, 4.0 and 6.0 m/s at the equivalence ratios of 0.4, 0.5 and 0.6, respectively. Comparing these values with Fig. 4, one can see that the micro-combustor with a bluff body greatly extends the stable combustion range of hydrogen/air mixture. In addition, it is seen from Fig. 4 that the blow-off limit increases with the increase of the equivalence ratio. This is mainly because for lean hydrogen/air mixtures, the amount of heat release and chemical reaction rate increase with the equivalence ratio [34]. Consequently, the solid and gas temperatures can remain at a higher level for a larger equivalence ratio, as clearly shown in Fig. 5. Thus, the negative effect of heat losses on combustion stability can be reduced to some extent, which can be clearly seen from the contours of radical H, as shown in Fig. 6. From Fig. 6, it is evident that the chemical reaction intensity is enhanced at a higher equivalence ratio.

To help analyzing the mechanism of flame stabilization by the bluff body, contours of flow field and radical H for different inlet velocities at the same equivalence ratio of 0.5 are illustrated in Figs. 7 and 8 , respectively. It can be seen from Fig. 7a

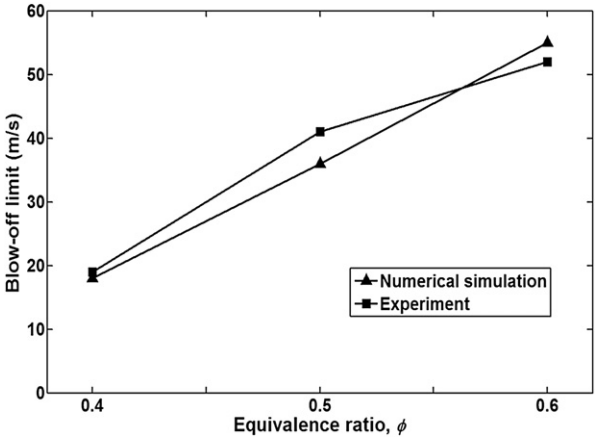

Fig. 4 – Experimental and numerical results of blow-off limits for different equivalence ratios.

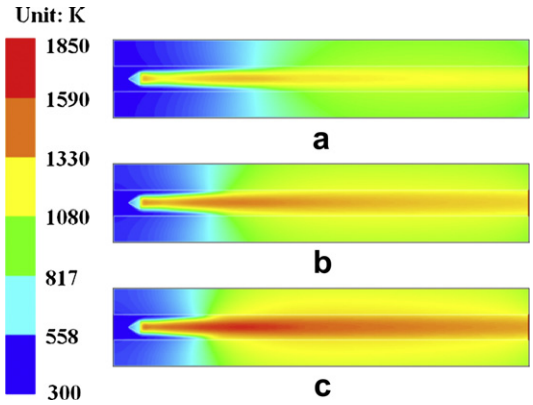

Fig. 5 – Numerical results of temperature fields for different equivalence ratios at the inlet velocity of 10 m/s: (a) $\phi = 0.4$, (b) $\phi = 0.5$, (c) $\phi = 0.6$.

that a small recirculation zone is formed behind the bluff body. Owing to the existence of the recirculation zone, a stable reaction zone (region of high H concentration) is sustained and thus the flame is anchored by the bluff body, as shown in Fig. 8a. With the increment of the inlet velocity, both the recirculation zone and reaction zone are prolonged (see Figs. 7b and 8b). However, with a further increase of the inlet velocity, although the recirculation zone is continuously prolonged and enlarged, the middle of the reaction zone becomes thinner and tends to be split into two parts, as indicated by an arrow in Fig. 8c. Finally, flame is no longer able to be sustained at even larger velocities because the reaction zone behind the bluff body is too small, i.e., blow-off occurs.

4.3. *Effects of the equivalence ratio and inlet velocity on the exhaust gas temperature*

Fig. 9 illustrates the variation tendencies of the measured exhaust gas temperature versus the inlet velocity at different equivalence ratios. From this figure, it can be seen that the exhaust gas temperature increases with the equivalence ratio when the inlet velocity is fixed. The reason is that when the equivalence ratio is larger, more combustion heat is released which leads to a higher temperature level in the combustor (see Fig. 5). As a result, the exhaust gas temperature is also

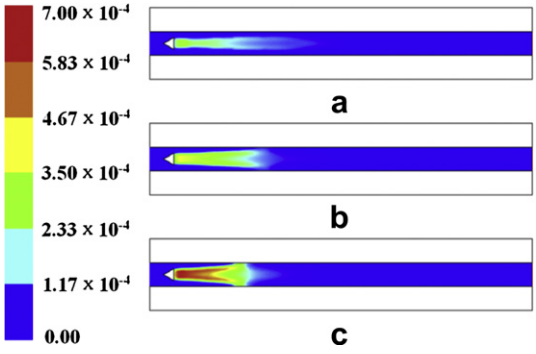

Fig. 6 – Numerical results of mass fraction contours of radical H for different equivalence ratios at the inlet velocity of 10 m/s: (a) $\phi = 0.4$, (b) $\phi = 0.5$, (c) $\phi = 0.6$.

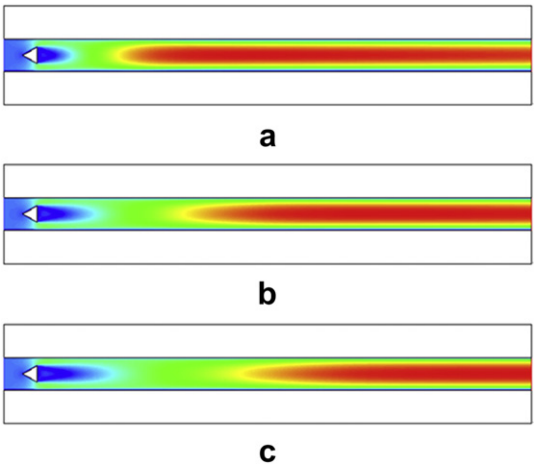

Fig. 7 – Numerical results of flow fields in the combustor for different inlet velocities at the equivalence ratio of 0.5: (a) V_{in} = 10 m/s, (b) V_{in} = 20 m/s, (c) V_{in} = 30 m/s. The blue region indicates the recirculation zone, while the red region indicates the high velocity zone of burned gas. [For interpretation of color referred in this figure legend, the reader is referred to web version of the article.]

raised. Moreover, it is noted that the exhaust gas temperature increases first and then decreases with the increasing inlet velocity. This means that the exhaust gas temperature reaches a peak at a moderate inlet velocity. The corresponding inlet velocities for the equivalence ratios of 0.4, 0.5 and 0.6 are 7.0 m/s, 23.0 m/s and 23.0 m/s, respectively. Obviously, this value depends on many factors, including the equivalence ratio, heat losses, and combustion efficiency. The last one will be discussed in the following section.

4.4. *Effects of the equivalence ratio and inlet velocity on combustion efficiency*

Fig. 10 depicts the numerical results of combustion efficiency against inlet velocity under different equivalence ratios. It is seen from Fig. 10 that even the lowest combustion efficiency is larger than 0.96, which demonstrates that relatively complete conversion can be achieved in this micro-combustor. Moreover, one can see that the combustion efficiency increases first and

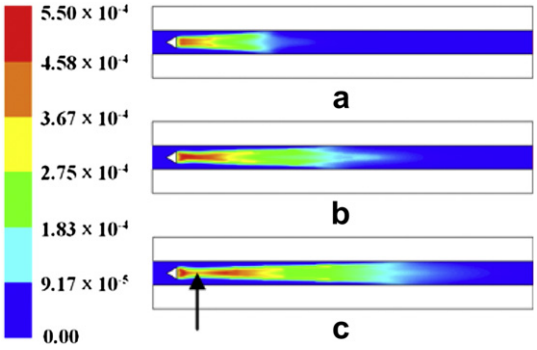

Fig. 8 – Numerical results of mass fraction contours of radical *H* for different inlet velocities at the equivalence ratio of 0.5: (a) V_{in} = 10 m/s, (b) V_{in} = 20 m/s, (c) V_{in} = 30 m/s.

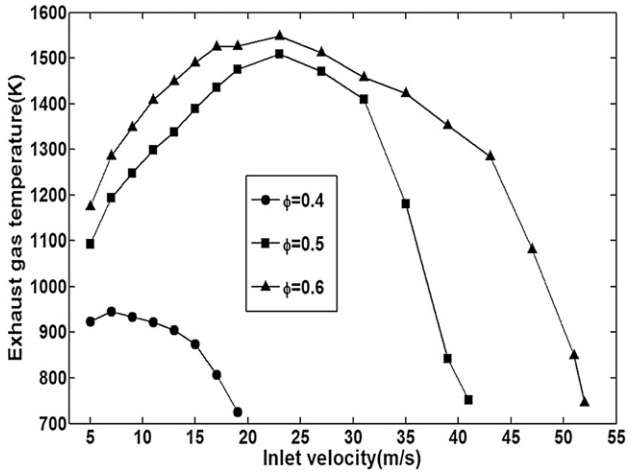

Fig. 9 – Experimental data of exhaust gas temperature versus inlet velocity for different equivalence ratios.

then decreases with the increasing inlet velocity when the equivalence ratio is fixed. This non-monotonic variation characteristic is like that of the exhaust gas temperature (see Fig. 9). Similarly, the inlet velocity corresponding to the maximum combustion efficiency depends on the equivalence ratio, flame temperature, and heat losses. Meanwhile, the corresponding inlet velocities reaching a maximum efficiency are 8.0 m/s, 10.0 m/s and 15.0 m/s for equivalence ratios of 0.4, 0.5 and 0.6, respectively. This means that the highest combustion efficiency reaches at a smaller velocity when the equivalence ratio is lower. Furthermore, for the equivalence ratio of 0.5, the combustion efficiency can maintain above 0.99 under most inlet velocities. This indicates that a moderate equivalence ratio is beneficial to achieve a relatively complete combustion.

4.5. *Effect of the inlet velocity on the wall temperature profile*

The effect of inlet velocity on the outer wall temperature profile is numerically investigated and the results are demonstrated in Fig. 11 for the same equivalence ratio of 0.5.

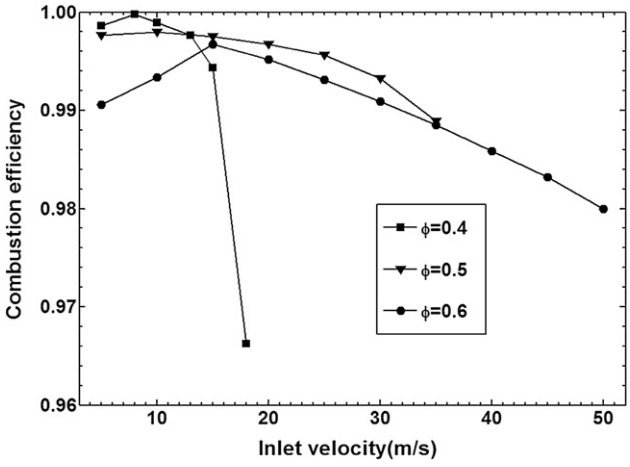

Fig. 10 – Numerical results of combustion efficiency versus inlet velocity for different equivalence ratios.

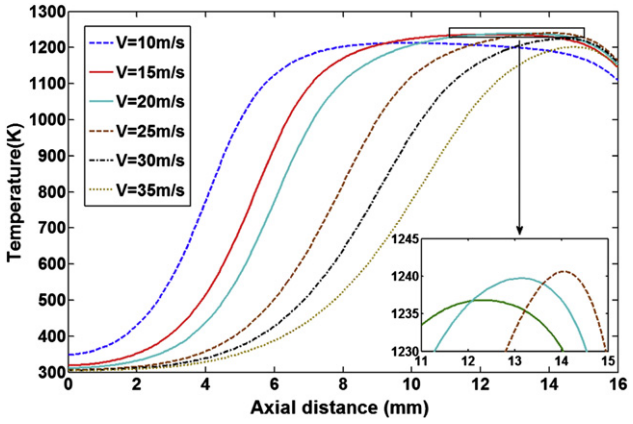

Fig. 11 – Numerical results of outer wall temperature profiles for different inlet velocities at the equivalence ratio of 0.5.

From Fig. 11, several characteristics can be observed. First, it is seen that the segment of high wall temperature shifts downstream with the increasing inlet velocity. This is because the reaction zone is prolonged and the high temperature zone is pushed farther downstream as the inlet velocity is increased, as have been shown in Fig. 8. Second, it is noted from Fig. 11 that the upstream wall temperature is higher at a lower inlet velocity than that at a higher inlet velocity. There are two main reasons for this phenomenon. On the one hand, the high temperature burned gases in the combustor chamber is pushed farther downstream under high velocity conditions, which reduces the convection heat transfer between the fluid and solid wall in the upstream; On the other hand, as the segment of high wall temperature shifts downstream with the increasing inlet velocity, the amount of heat conduction through the solid wall to the upstream is reduced. Therefore, under a lower velocity condition, the wall temperature level of the upstream is higher than that under a larger velocity condition. Finally, from the enlarged drawing in Fig. 11, one can see that the highest wall temperature appears at the inlet velocity of 25 m/s. This is expected to be determined by many factors, such as the gaseous temperature distribution, heat losses, combustion efficiency, wall material, etc.

5. Conclusions

Combustion characteristics of lean hydrogen/air mixture in a micro-combustor with a bluff body were investigated through experiment and simulation. Effects of the inlet velocity and equivalence ratio on the blow-off limit, combustion efficiency, exhaust gas temperature and outer wall temperature profile were examined. The results show that the blow-off limit is obviously extended as compared with that of the micro-combustor without a bluff body. Meanwhile, the blow-off limit increases as the equivalence ratio is increased from 0.4 to 0.6. Moreover, comparatively high combustion efficiency can be maintained over the whole combustible velocity range at a moderate equivalence ratio. The inlet velocity also exerts a significant effect on the combustion characteristics. With the increase of inlet velocity, flame was prolonged and thus the high temperature zone is pushed toward the downstream of the combustor chamber. However, the exhaust gas temperature, combustion efficiency, and outer wall temperature reaches a peak value at a moderate inlet velocity under a fixed equivalence ratio. These variation tendencies indicate that the combustion characteristics are determined by many factors and their complicated interactions.

Acknowledgments

This work was supported by the Natural Science Foundation of China (Grant Nos. 51076054 and 51276073) and the Foundation of Key Laboratory of Low-grade Energy Utilization Technologies and Systems, Chongqing University, China.

REFERENCES

[1] Dunn-Rankin D, Leal EM, Walther DC. Personal power systems. Prog Energy Combust Sci 2005;31:422–65.
[2] Fernandez-Pello AC. Micro-power generation using combustion: issues and approaches. Proc Combust Inst 2002; 29:883–99.
[3] Maruta K. Micro and mesoscale combustion. Proc Combust Inst 2011;33:125–50.
[4] Ju YG, Maruta K. Microscale combustion: technology development and fundamental research. Prog Energy Combust Sci 2011;37:669–715.
[5] Maruta K, Kataoka T, Kim NI, Minaev S, Fursenko R. Characteristics of combustion in a narrow channel with a temperature gradient. Proc Combust Inst 2005;30:2429–36.
[6] Richecoeur F, Kyritsis DC. Experimental study of flame stabilization in low Reynolds and Dean number flows in curved mesoscale ducts. Proc Combust Inst 2005;30:2419–27.
[7] Jackson TL, Buckmaster J, Lu Z, Kyritsis DC, Massa L. Flames in narrow circular tubes. Proc Combust Inst 2007;31:955–62.
[8] Pizza G, Frouzakis CE, Mantzaras J, Tomboulides AG, Boulouchos K. Dynamics of premixed hydrogen/air flames in microchannels. Combust Flame 2008;152:433–50.
[9] Fan Y, Suzuki Y, Kasagi N. Experimental study of micro-scale premixed flame in quartz channels. Proc Combust Inst 2009; 32:3083–90.
[10] Minaev S, Maruta K, Fursenko R. Nonlinear dynamics of flame in a narrow channel with a temperature gradient. Combust Theory Model 2007;11:187–203.
[11] Minaev S, Sereshchenko E, Fursenko R, Fan AW, Maruta K. Splitting flames in a narrow channel with a temperature gradient in the walls. Combust Explos Shock Waves 2009;45: 119–25.
[12] Fan AW, Minaev S, Sereshchenko E, Tsuboi Y, Oshibe H, Nakamura H, et al. Propagation dynamics of splitting flames in a heated microchannel. Combust Explos Shock Waves 2009;45:245–50.
[13] Nakamura H, Fan AW, Minaev S, Sereshchenko E, Fursenko R, Tsuboi Y, et al. Bifurcations and negative propagation speeds of methane/air premixed flames with repetitive extinction and ignition in a heated microchannel. Combust Flame 2012;159:1631–43.
[14] Kumar S, Maruta K, Minaev S. Pattern formation of flames in radial microchannels with lean methane-air mixtures. Phys Rev E 2007;75:016208.
[15] Kumar S, Maruta K, Minaev S. On the formation of multiple rotating pleton-like flame structures in radial microchannels

with lean methane–air mixtures. Proc Combust Inst 2007;31:3261–8.
[16] Fan AW, Minaev S, Kumar S, Liu W, Maruta K. Regime diagrams and characteristics of flame patterns in radial microchannels. Combust Flame 2008;153:479–89.
[17] Fan AW, Minaev S, Sereshchenko E, Fursenko R, Kumar S, Liu W, et al. Experimental and numerical investigations of flame pattern formations in a radial microchannel. Proc Combust Inst 2009;32:3059–66.
[18] Zamashchikov V, Tikhomolov E. Sub-critical stable hydrogen–air premixed laminar flames in micro gaps. Int J Hydrogen Energy 2011;36(14):8583–94.
[19] Kim NI, Aizumi S, Yokomori T, Kato S, Fujimori T, Maruta K. Development and scale effects of small Swiss-roll combustors. Proc Combust Inst 2007;31:3243–50.
[20] Jejurkar SY, Mishra DP. Flame stability studies in a hydrogen–air premixed flame annular microcombustor. Int J Hydrogen Energy 2011;36:7326–38.
[21] Li J, Chou SK, Li ZW, Yang WM. Experimental investigation of porous media combustion in a planar micro-combustor. Fuel 2010;89:708–15.
[22] Jiang LQ, Zhao DQ, Wang XH, Yang WB. Development of a self-thermal insulation miniature combustor. Energy Convers Manage 2009;50:1308–13.
[23] Yang WM, Chou SK, Shu C, Li ZW, Xue H. Combustion in micro-cylindrical combustors with and without a backward facing step. Appl Therm Eng 2002;22:1777–87.
[24] Pan JF, Huang J, Li DT, Yang WM, Tang WX, Xue H. Effects of major parameters on micro-combustion for thermophotovoltaic energy conversion. Appl Therm Eng 2007;27:1089–95.
[25] Chen GB, Chen CP, Wu CY, Chao YC. Effects of catalytic walls on hydrogen/air combustion inside a micro-tube. Appl Catal A Gen 2007;332:89–97.
[26] Boyarko GA, Sung CJ, Schneider SJ. Catalyzed combustion of hydrogen–oxygen in platinum tubes for micro-propulsion applications. Proc Combust Inst 2005;30:2481–8.
[27] Choi WY, Kwon SJ, Shin H. Combustion characteristics of hydrogen–air premixed gas in a sub-millimeter scale catalytic combustor. Int J Hydrogen Energy 2008;33:2400–8.
[28] Zhang YS, Zhou JH, Yang WJ, Liu MS, Cen KF. Effects of hydrogen addition on methane catalytic combustion in a micro-tube. Int J Hydrogen Energy 2007;32:1286–93.
[29] Wang F, Zhou J, Wang GQ, Zhou XJ. Simulation on thermoelectric device with hydrogen catalytic combustion. Int J Hydrogen Energy 2012;37:884–8.
[30] Zhong BJ, Yang F. Characteristics of hydrogen-assisted catalytic ignition of n-butane/air mixtures. Int J Hydrogen Energy 2012;37:8716–23.
[31] Nair S, Lieuwen T. Near-blowoff dynamics of a bluff-body stabilized flame. J Propul Power 2007;23:421–8.
[32] Brundage AL, Donaldson AB, Gill W, Kearney SP, Nicolette VF, Yilmaz N. Thermocouple response in fires, part 1: considerations in flame temperature measurements by a thermocouple. J Fire Sci 2011;29:195–211.
[33] Kuo CH, Ronney PD. Numerical modeling of non-adiabatic heat-recirculating combustors. Proc Combust Inst 2007;31:3277–84.
[34] Turns SR. An introduction to combustion. 2nd ed. New York: McGRAW-Hill; 2000.
[35] Hua J, Wu M, Kumar K. Numerical simulation of the combustion of hydrogen–air mixture in micro-scaled chambers. Part I: fundamental study. Chem Eng Sci 2005;60:3497–506.
[36] Ma QF, Fang RS, Xiang LC. Handbook of thermo-physical properties. Bejing: China Agricultural Machinery Press; 1986 (in Chinese).
[37] Li J, Zhao ZW, Kazakov A, Dryer FL. An updated comprehensive kinetic model of hydrogen combustion. Int J Chem Kinet 2004;36:1–10.
[38] Kee RJ, Grear JF, Smooke MD, Miller JA. A Fortran program for modeling steady laminar one-dimensional premixed flames. Sandia National Laboratories Report SAND85-8240; 1985.
[39] Holman JP. Heat transfer. 9th ed. London: McGraw Hill; 2002.
[40] Fluent 6.3 user's guide. Lebanon, New Hampshire: Fluent Inc.; 2006.